Applied Surface Science 435 (2018) 718–732

Contents lists available at ScienceDirect

Applied Surface Science

journal homepage: www.elsevier.com/locate/apsusc

Full length article

# Catalyst-free fabrication of novel ZnO/CuO core-Shell nanowires heterojunction: Controlled growth, structural and optoelectronic properties

Muhammad Arif Khan[a,b,*], Yussof Wahab[c], Rosnita Muhammad[b], Muhammad Tahir[d], Samsudi Sakrani[a,b]

[a] Centre for Sustainable Nanomaterials (CSNano) Ibnu Sina Institute for Scientific and Industrial Research, Universiti Teknologi Malaysia, Skudai, 81310 Johor, Malaysia
[b] Nanotechnology Research Alliance, Department of Physics, Faculty of Science, Universiti Technologi Malaysia, Skudai, 81310 Johor, Malaysia
[c] Razak School of Engineering and Advanced Technology Universiti Technologi Malaysia Kuala Lumpur Level 7, Razak Tower Jalan Semarak, 54100 Kuala Lumpur, Malaysia
[d] Chemical Reaction Engineering Group (CREG), Faculty of Chemical and Energy Engineering, Universiti Teknologi Malaysia, Skudai, 81310 Johor, Malaysia

ARTICLE INFO

*Article history:*
Received 5 June 2017
Received in revised form 9 November 2017
Accepted 9 November 2017
Available online 14 November 2017

*Keywords:*
Catalyst-free
ZnO/CuO core-shell NW arrays
C-AFM
p-n junction
Band offset
Type-II band alignment

ABSTRACT

Development of controlled growth and vertically aligned ZnO/CuO core-shell heterojunction nanowires (NWs) with large area by a catalyst free vapor deposition and oxidation approach has been investigated. Structural characterization reveals successful fabrication of a core ZnO nanowire having single crystalline hexagonal wurtzite structure along [002] direction and CuO nanostructure shell with thickness (8–10 nm) having polycrystalline monoclinic structure. The optical property analysis suggests that the reflectance spectrum of ZnO/CuO heterostructure nanowires is decreased by 18% in the visible range, which correspondingly shows high absorption in this region as compared to pristine ZnO nanowires. The current-voltage (*I–V*) characteristics of core-shell heterojunction nanowires measured by conductive atomic force microscopy (C-AFM) shows excellent rectifying behavior, which indicates the characteristics of a good p-n junction. The high-resolution transmission electron microscopy (HRTEM) has confirmed the sharp junction interface between the core-shell heterojunction nanowire arrays. The valence band offset and conduction band offset at ZnO/CuO heterointerfaces are measured to be $2.4 \pm 0.05$ and $0.23 \pm 0.005$ eV respectively, using X-ray photoelectron spectroscopy (XPS) and a type-II band alignment structure is found. The results of this study contribute to the development of new advanced device heterostructures for solar energy conversion and optoelectronics applications.



## 1. Introduction

Core–shell nanowires (NWs) structures are found to be promising materials for their novel applications and have drawn much attention for developing new challenging devices due to their high interfacial area, allowing for more electron–hole formation or recombination [1–3]. ZnO has been considered as a versatile and core material due to easiness of growing it in the nanostructure form [4], direct large band gap of 3.37 eV, large exciton having binding energy 60 mV [5] and highly-developed fabrication techniques [6]. ZnO material represents the richest family of nanostructures, due to which it is used as a promising substrate materials for various applications. These promising features enable the fabrication of various nanodevices such as field effect transistors, new generation of solar cells, bio- and chemical sensors, bio-imaging, drug delivery and light-emitting diodes (LEDs) using various types of ZnO nanostructures [7–10]. However, successful commercial application of ZnO NWs based devices requires a detailed understanding of the control growth, structural quality, and specific properties related to the application purpose. Depending upon the growth method, the as-grown ZnO NWs invariably contain several surface defects, for example, inefficient UV emission for optoelectronic applications and low electronic conductivity for device application [6,11]. The surface modification of ZnO nanowires and its controlled morphology play important role to change the physical properties

* Corresponding author. Present address: Centre for Sustainable Nanomaterials (CSNano) Ibnu Sina Institute for Scientific and Industrial Research, Universiti Teknologi Malaysia, Skudai, Johor 81310, Malaysia.
*E-mail addresses:* marifkhan_qau@hotmail.com, akmuhammad6@live.utm.my (M.A. Khan).

https://doi.org/10.1016/j.apsusc.2017.11.071
0169-4332/

(electrical, optical and magnetic properties) for enhanced application at nanoscale regime [12,13]. Core-shell heterojunction NWs is a better technique to enhance and control the properties of the materials [14]. The shell development or formation of CuO to vertically aligned ZnO nanowires offers an attractive platform for solar cells because of attractive p-type material with semiconducting properties of having good absorption coefficient and direct band gap (1.2 eV) [15]. The intrinsic, stable, direct band gap and p-type nature properties make CuO a good candidate for electrical, optical, sensing, catalyst, photovoltaic and optoelectronic devices [16]. Consequently, the fabrication of core-shell heterojunction nanowires has attracted much interest for optoelectronic and nanoelectronic device applications. This is because these core-shell nanowires heterojunctions are expected to have improved charge collection efficiency because of the lower interval and higher contact area between the p-type and n-type materials. In addition, development of favorable radial p-n junctions of *n*-ZnO/p-CuO core-shell nanowires heterojunction at the nanostructure interface could enhance the charge collection, reduce the defect states at the interface and thus bestow improved performance in nanoelectronic devices. The fabrication of vertically-aligned and large-area core-shell nanowires heterojunction with high aspect ratio can be considered as an ideal nanoscale heterostructure for potential applications in nano-optoelectronic.

Herein, we report for the first time a catalyst-free fabrication of novel ZnO/CuO core-shell nanowires heterojunction, its controlled growth, structural, optoelectronic properties and band offsets measurements at ZnO/CuO heterointerfaces. The vertically aligned *n*-ZnO/p-CuO core-shell heterojunction nanowire (NW) arrays were successfully fabricated on an n-type Si substrate using modified thermal chemical vapor deposition (CVD) assisted physical vapor deposition (PVD) techniques/sputtering followed by thermal oxidation under controlled growth conditions. The structure, growth mechanism, optical and electrical properties of the vertically aligned ZnO/CuO core-shell heterojunction nanowires were studied in detail by different characterization techniques. The band offsets at ZnO/CuO heterointerfaces were measured by X-ray photoelectron spectroscopy (XPS). The purpose of this study is to investigate the ZnO surface properties and to develop new advanced device heterostructure of ZnO/CuO core-shell heterojunction NWs for optoelectronic applications. The advantages of the thermal CVD in conjunction with PVD of high vacuum sputtering followed by thermal oxidation are being used to produce high purity, high-performance and vertically-aligned large-area *n*-ZnO/p-CuO core-shell nanowires heterojunction. The absence of a particle (catalyst free) may, however, be an advantage as the particle is passive during radial growth and may present a complication. Also, this study provides the controlled growth mechanism, due to which it is possible to control crystal structure, surface morphologies and orientation of the core-shell nanowires. Finally, the mechanisms for each step are documented with the detailed characterization analysis.

## 2. Experimental section

### 2.1. CVD growth of vertical aligned ZnO NWs

Large scale fabrication of vertically aligned ZnO nanowire arrays were executed in a horizontal quartz tube furnace reactor of inner diameter 43 mm and length 450 mm by a thermal chemical vapor deposition (CVD), where the growth parameters like gas flow rate (oxygen and argon), pressure inside the quartz tube, temperature and time were well controlled. In a sample preparation step, first cut two Si substrates ($1 \times 1\,cm^2$) using a diamond cutter followed by ultrasonic wash in acetone, alcohol and de-ionized water for 30 min each and dry under nitrogen atmosphere. Alumina boat containing 0.5 g pure Zn powder in a metallic form (99.99% Alfa Aldrich) was kept in the middle region of a quartz tube of thermal CVD system. Si substrates were kept on a flat alumina plate in the quartz tube downward region, where the temperature was about 760 °C, as shown in Fig. 1a. The distance between the source boat containing Zn powder and Si substrates was around 5 cm. The tube was sealed and the pressure inside the quartz tube reduced to $5 \times 10^{-2}$ torr using two-step high-speed vacuum pump. The furnace was heated to temperature of 800 °C for 2 h using a furnace heating rate at 10 °C $min^{-1}$. Pure argon (Ar) gas with a constant flow of 180 mL/min regulated by MFC was supplied to the tube furnace during the entire process at room temperature. Oxygen ($O_2$) gas of a high purity was supplied at a flow rate of 20 mL/min into the tube furnace of thermal chemical vapor deposition system, while keeping all operating parameters at steady state. The pressure was maintained about 8 Torr inside the quartz tube furnace for nanowires formation and it was precisely measured by digital vacuum gauge. After the completion of growth process, when the temperature of the furnace reached its normal room temperature, a product of thin layer having white or gray matter was obtained on the top surface of Si substrates. The schematic of new modified Thermal CVD is shown in Fig. 1.

### 2.2. Growth of Cu nano-shell onto the as-grown ZnO nanowires

After the fabrication of vertically aligned ZnO nanowire arrays, the as-synthesized ZnO NW arrays taken as a template were then shifted to high vacuum sputtering for Cu nanofilm deposition. The Cu nanofilm of thickness 20 nm ± 2 under high vacuum $5 \times 10^{-5}$ mbar was used to deposit onto the as-grown ZnO nanowires using a Dual Target Sputtering System (Q300T D). The chamber of the sputtering system having outside diameter of 300 mm and height of 127 mm is fully integrated with Dual channel film thickness monitor (FTM) to control the thickness of nanofilms. During the deposition of copper nanofilm, a high purity 4N (99.99%) Cu as the sputtering target was used, while keeping the optimized sputtering deposition time 4 min, sputtering current 60 mA and substrate and target distance 5 cm.

### 2.3. Growth of n-ZnO/p-CuO core-shell nanowire heterojunction

After successful deposition of Cu nanostructure shell onto the as-grown ZnO NWs, ZnO/Cu nanowires were brought into the CVD Tube Furnace for thermal oxidation in rich oxygen and the sample was kept in the middle portion of a quartz tube furnace on a flat alumina boat. The tube was sealed again and the pressure inside the quartz tube reduced to $5 \times 10^{-2}$ torr using two-step high-speed vacuum. The furnace was heated to temperatures 400 °C for 1 h using a furnace heating rate of 10 °C $min^{-1}$. Pure Ar gas with a constant flow was supplied to the tube furnace at 140 mL/min flow rate during the entire process to its room temperature. High purity $O_2$ gas was supplied at a flow rate 45 mL/min into the tube furnace of thermal CVD system, while keeping all operating parameters at steady state. The pressure was maintained about 75 Torr inside the quartz tube in the presence of rich oxygen, with the temperature of the furnace kept constant. After the completion of growth process, when the temperature of the furnace was naturally cooled until it reached room temperature, the *n*-ZnO/p-CuO core-shell heterojunction nanowires were obtained. The detailed growth mechanism and fabrication illustration of the core-shell heterojunction nanowires is given in Fig. S1 (Supporting information).

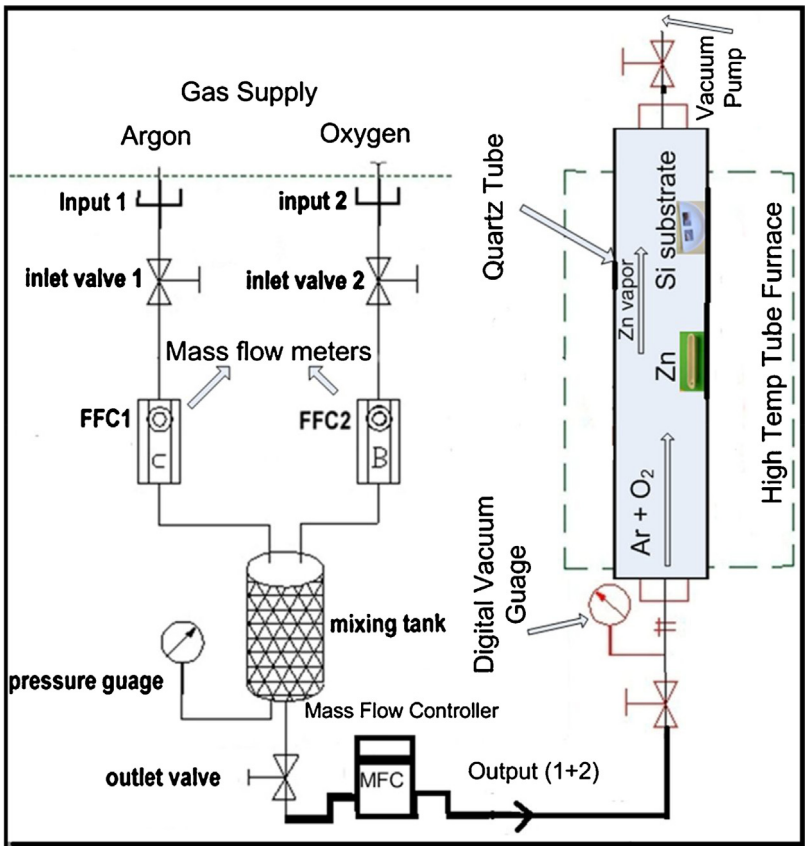


**Fig. 1.** Schematic of thermal CVD.

### 2.4. Characterization

The morphological study of the as grown ZnO nanowires and their core-shell (ZnO/CuO) heterojunction nanowires arrays was characterized by SU8020 Hitachi FE-SEM machine at 15 kV. The crystal quality of the as grown ZnO NWs and ZnO/CuO core-shell heterojunction nanowires was studied by Bruker AXS D5005 X-ray diffraction (XRD) equipped with Cu having Kα radiation at λ = 1.54056 Å using 40 kV generator voltage and 30 mA current. Transmission electron microscopy (TEM) is operated using TECNAI G2 20 S-TWIN, FEI electron microscope working of 200 kV (accelerating voltage). Transmission electron microscopy was used to characterize the single ZnO nanowire and ZnO/CuO core-shell heterojunction nanowire for their lattice spacing, interface junction, directions and plane. For the TEM measurements, the nanowires grown on the Si wafer were cut into small sizes and then put in the clean plastic centrifuge test tube containing acetone for the nanowires extraction. The centrifuge test tubes were kept in small glass beaker containing a small amount of water for sonication purpose using Ultrasonic cleaner for 45 min at 25 °C. A microlitre pipette was used to pick-up a drop of sample solution containing the nanowires and is transferred on a nickel TEM grid which is covered with a thin layer of amorphous carbon. The grid sample was held for 2 min and then blotting paper was used to remove the extra solution in order to dry the grid before the TEM measurement. The EDX spectrometer, which is fixed with the transmission electron microscopy instrument, is used to trace the elemental composition of core-shell heterojunction nanowires. TEM is also performed in diffraction modes, such as selected area electron diffraction (SEAD). X-ray photoelectron spectrometer was used for the study of core-level spectra and valance band spectra. All XPS spectra samples were characterized using Shimadzu Kratos Axis Ultra DLD system of X-ray photoelectron spectroscopy, which worked at 15 kV and 10 mA and were measured with the reference to the carbon 1s (C 1s) peak at 284.60 eV. The sample used for XPS analysis was a dry solid sample of size 1 cm x 1 cm and from the XPS analysis, the number of electrons is plotted as a function of binding energy to produce survey spectra. Additional structural information of pure ZnO NW arrays and ZnO/CuO core-shall hetero-structure NW arrays obtained by HORIBA LabRAM HR Raman spectrometer at room temperature having range of 50–1100 $cm^{-1}$. The UV–vis Reflectance spectra were analyzed for the prepared samples at room temperature using Shimadzu UV-1601PC spectroscopy instrument.

### 2.5. Testing for p-n junction using conductive AFM

Electrical measurements of *n*-ZnO/p-CuO core-shell heterojunction NW arrays were studied by conductive AFM in contact mode at atmospheric room temperature using an SPA 300HV SPM Unit measurement system with a voltage range of −10 to +10 V from Seiko Instrument Inc., Japan. To contact the NWs, the conductive AFM (C-AFM) used the conductive tip as a movable electrode. The silicon cantilever tip having diameter with a 100 nm was covered by a Rhodium (Rh) thin layer, which is a chemical inert transition metal and is a member of the platinum group. The spring constant of the measurement system was 13 N/m and the scanning rate of the frequency for the current analysis was about 1 Hz. For capturing smoothest topography and current imaging, the movement of the tip frequency of about 1 Hz was applied during the scanning. For the current-voltage measurement of *n*-ZnO/p-CuO core-shell heterojunction NWs on n-type Si (100) substrate, the current analysis was studied when the electrical contact was formed between the conductive AFM tip and one of the core-shell nanowire tips.

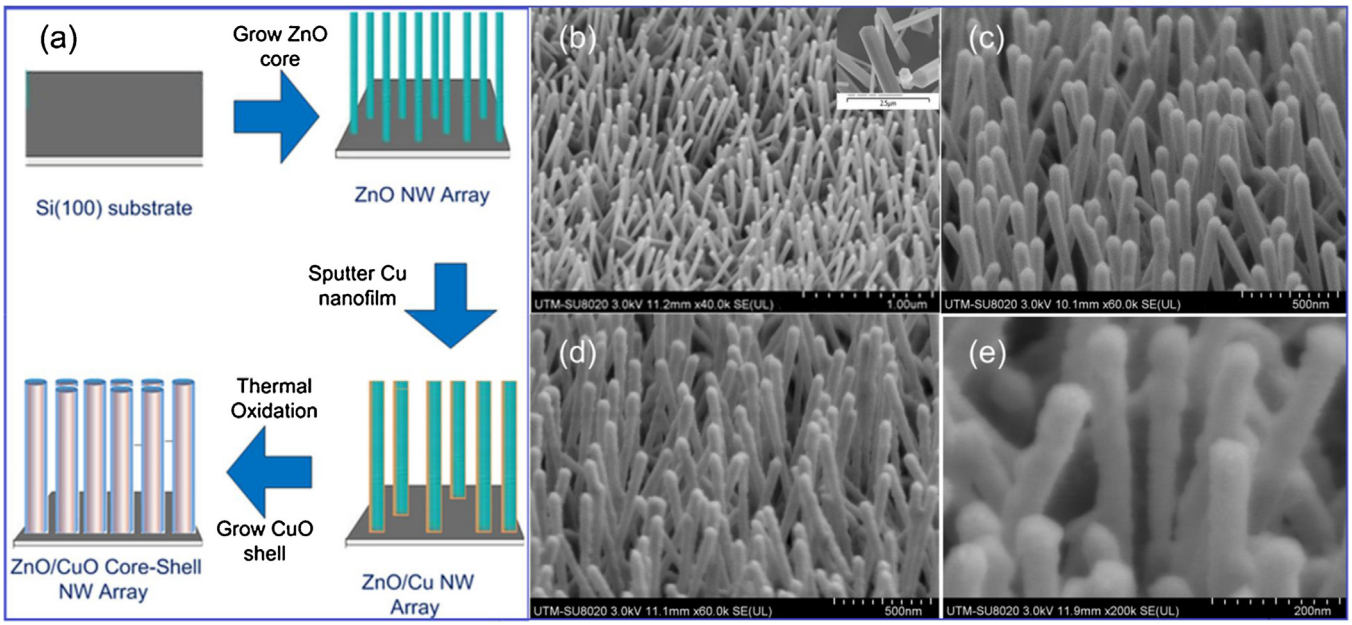


**Fig. 2.** (a) Schematic illustration and growth process of vertically aligned ZnO/CuO Core-Shell heterojunction nanowires (b) FESEM image of pure ZnO NW arrays on n-type Si (100) substrate (c) ZnO/Cu NW arrays after deposition of copper (Cu) by sputtering for optimized time and current (i.e. sputtering time 4 min and sputtering current 60 mA) (d) and (e) FESEM images of the *n*-ZnO/p-CuO core-shell heterojunction nanowires at two different magnifications fabricated by thermal oxidation of ZnO/Cu NW arrays at temperature 400 °C for time 1 h and at pressure inside the quartz tube of 75 Torr, with oxygen flow rate of 45 mL/min.

## 3. Results and discussion

### 3.1. Morphological characteristics

Fig. 2a represents the schematic fabrication illustration of vertically aligned large-area *n*-ZnO/p-CuO core-shell heterojunction nanowires. Fig. 2b shows the FESEM image of pure ZnO nanowire arrays grown on n-type Si (100) substrate using thermal CVD technique. The inset in Fig. 2b is an enlarged image of ZnO nanowire of hexagonal shape and a smooth surface having diameter in the range of 35–45 nm and a length of about 700–1300 nm, respectively. The ZnO NWs shown in the enlarged FESEM image has a high density and the tip of NW arrays shows that there are no metal catalyst particles on the nanowire, indicating the growth mechanism to be a vapor-solid (VS) mechanism. After a deposition of $20 \pm 2$ nm Cu nanofilm by sputtering on as grown ZnO NW arrays under a well-controlled condition, the NWs diameter became in the range of 50–65 nm, whereas the obtained ZnO/Cu NW arrays retained their original reflection. The ZnO/Cu NWs after deposition of Cu nanofilm by sputtering is shown in Fig. 2c and it is clearly revealed that copper has been successfully deposited as a thin nanofilm on the surface of ZnO nanowires arrays. Fig. 2d and e are the FESEM images of the *n*-ZnO/p-CuO core-shell heterojunction nanowires at two different magnifications. The core-shell heterostructure of ZnO/CuO nanowire arrays are obtained by thermal oxidation of ZnO/Cu NW arrays in the presence of rich oxygen in CVD Tub Furnace under controlled operating conditions.

The growth progress and morphologies barrier of the shell layer for the ZnO/CuO core-shell nanowires structure were also studied using the effect of pressure and oxygen flow gas inside a quartz tube furnace using thermal chemical vapor deposition system. The shell layer of CuO nanostructure is affected by changing the pressure of oxygen gas and oxygen flow rate though thermal oxidation [17]. At low pressure 50 Torr and low oxygen 25–30 mL/min flow rate, the CuO nanostructure shell were not grown uniformly on the core ZnO NWs surface as shown by the FESEM image supported by the XRD result in Fig. S2a and Fig. S2b (Supporting Information), respectively. When pressure inside the quartz tube increased to 75 Torr, and oxygen flow rate increased to 45 mL/min, the quality of the heterostructure nanowires became much better and the CuO nanostructure shell were grown uniformly on the core ZnO nanowires surface as shown by the FESEM image supported by the XRD result in Fig. S2c and Fig. S2d (Supporting Information), respectively. As a result of higher pressure and higher flow rate of oxygen, the oxidation rate of ZnO/Cu is increasing and very rapid CuO material fill-in between the adjacent ZnO-Cu nanowires top, middle and bottom portion is nearly uniform, leading to good quality of *n*-ZnO/p-CuO core-shell NW arrays. In addition, the flow rate of higher oxygen during thermal oxidation plays important role to create an electric field between oxygen (O) ion and copper (Cu) ion. This is due to thermionic emission, as electrons will diffuse through oxidant and Cu ion will migrate to form the CuO thin layer since copper diffuses much faster than oxygen. At low pressure and low oxygen flow rate, however, the oxidation rate of ZnO/Cu only leads to dominate the top and some sides of the core-shell nanowires, forming ZnO/CuO core-shell nanowires, while the bottom portion of ZnO/Cu is still reaming and not oxidized because very limited amount of oxygen will be accessed at the bottom portion of nanowires. This evidence further proves that higher pressure and higher oxygen flow rate will favor a good thin shell layer of only CuO material for the vertically aligned *n*-ZnO/p-CuO core-shell heterojunction nanowires. The growth progress development of the shell layer for the vertical aligned ZnO/CuO core-shell heterojunction NWs structure for different sputtering deposition time are given in Fig. S3 and Table S1 (Supporting Information).

### 3.2. Structural characteristics analysis

Structural and compositional analysis of the pure ZnO nanowires and their core-shell heterostructure (ZnO/CuO) NWs were analyzed using XRD and XPS measurement techniques. The XRD structure of the vertical aligned ZnO nanowires arrays, ZnO/Cu NW arrays and heterostructure ZnO/CuO NW arrays are given in Fig. 3. In Fig. 3, the XRD spectrum (a) shows that the crystal structure of as synthesized ZnO nanowire arrays grown on Si substrate have hexagonal wurtzite with lattice parameters a = b = 0.324 nm

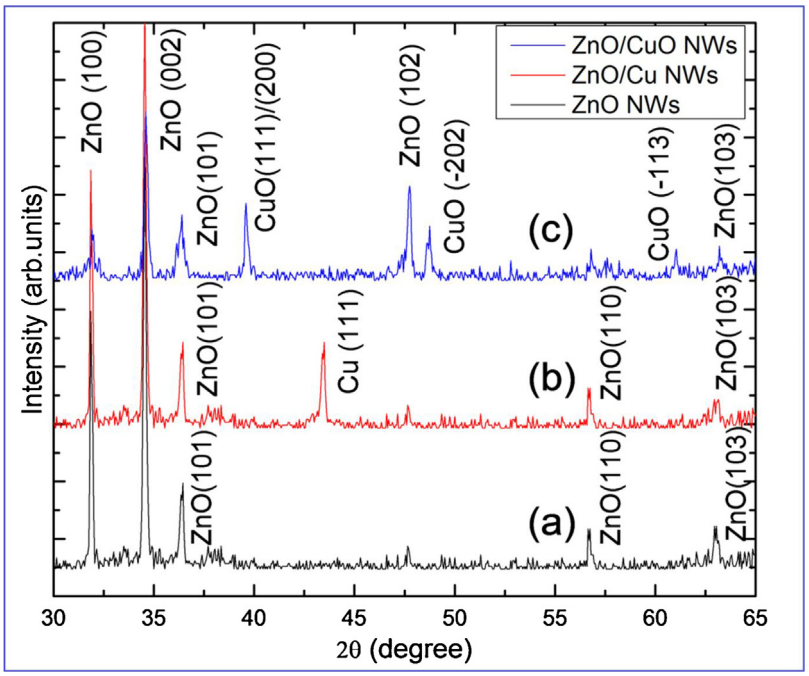


**Fig. 3.** X-ray Diffraction (XRD) spectrum (a) Pure ZnO nanowire arrays (b) ZnO/Cu core-shall nanowire arrays (c) ZnO/CuO core-shall NW arrays.

and c = 0.52 nm [18]. All samples of pure ZnO NWs gave similar XRD patterns, indicating high reproducibility of this method. Judging from the XRD pattern (JPCD 36-1451), no impurity pattern could be observed, which is opposite to the catalyst-assisted grown ZnO nanowires [19]. The prominent diffraction of (002) peaks is also a manifestation of preferential growth direction [002]. All these observations confirm that the products obtained are highly pure crystalline ZnO nanowire arrays with a preferential growth direction of [002]. In Fig. 3, the spectrum (b) shows the structure of ZnO/Cu nanowire arrays after deposition of Cu nanofilm by sputtering process. The structure of ZnO/Cu core-shell nanowire arrays shows all other peaks of ZnO NWs and only one copper (Cu) peak at 43.3°, which clearly corresponds to (111) plane having cubic structure with lattice parameters, a = b = c = 0.3615 nm of Cu (JCPD 04-0836). This evidence proves that copper has been successfully accumulated on the top surface of ZnO NW arrays. Spectra (c) in Fig. 3 reveals one broad peak at 38.8°, which corresponds to (111) and (200) planes of CuO (JPCD 89–5899) having monoclinic phase and lattice constant values of a = 0.4689 nm, b = 0.342 nm, c = 0.513 nm, while two other peaks at 48.85° and 61.85° correspond to (−202) and (−113) planes, respectively. After the thermal oxidation using pure oxygen at 400 °C for 1 h, the intensities of CuO peaks became stronger showing clear structure of ZnO/CuO core-shell heterojunction nanowire arrays. However, the peaks related to the other phases of copper like $Cu_2O$ and Cu metal were not noticed after thermal oxidation. This indicates that the fabrication of vertically aligned ZnO/CuO core-shell heterojunction nanowires was successfully achieved.

To determine the core-level spectra, valance band spectra, chemical composition and oxidation state of ZnO/CuO core-shall heterojunction nanowires, X-ray photoelectron spectroscopy (XPS) measurement was operated to study the representative samples. The details of measurement results of all XPS spectra samples are given in Fig. 4, where the binding energies of all XPS spectra samples were measured with standard value to the carbon 1s (C 1s) peak at 284.60 eV. In Fig. 4a, the complete profile spectra (survey scan) of ZnO/CuO core-shall heterojunction nanowires is shown, which shows clearly that the peaks related to copper (Cu), zinc (Zn), oxygen (O) and carbon (C) only. The wide survey scan analysis of XPS spectrum has confirmed that Cu, Zn, and O appeared on the surface of a sample. The Zn 2p spectrum of high-resolution is shown in Fig. 4d, which shows two intense peaks. The two intense peaks of Zn 2p, which are centered at 1021.92 and 1045.03 eV, represent the +2 oxidation state of Zn as $Zn^{2+}$ or ZnO. Furthermore, the estimated splitting of spin orbit between the two intensive peaks of Zn 2p is 23.07 eV indicates good agreement with the current literature value [20]. The oxidation states of Cu could be determined from Cu 2p XPS spectra given in Fig. 4c. The X-ray photoelectron spectrum of Cu 2p represents two major peaks, namely 2p3/2 and 2p1/2, and two shake-up satellite peaks. The spin-orbit lines of Cu 2p indicate two main peaks of 2p3/2 and 2p1/2 at 934.15 and 953.87 eV, respectively, while the shake-up satellite peaks are located at ~8 eV above the main peaks. Moreover, shakeup satellite peaks at 941.28 eV and 962.17 eV that could be assigned to the $3d^9$ shell of $Cu^{2+}$ ions are observed [21]. The binding energy values of Cu 2p, which correspond to the bivalent state of copper ($Cu^{2+}$) and the presence of satellite peaks, supports the evidence that Cu has been successfully oxidized to produce CuO [22,23]. Therefore, it is concluded that thermal oxidation of ZnO/Cu NW arrays successfully formed to produce ZnO/CuO core-shell heterojunction nanowires. The O1 s spectra in Fig. 4b also reveals an intense peak at 531.6 eV, which confirms that the binding energy of oxygen ion ($O^{2-}$) is well consisted with the metal oxide, whereas the shoulder peak at 529.9 eV has been assigned to the chemisorbed oxygen [24]. The XPS measurements have verified that the heterostructures consist of ZnO and CuO. These results are in good agreement with the XRD investigation.

### 3.3. TEM analysis of ZnO/CuO core-shell heterojunction nanowire

Fig. 5a shows TEM image of pure ZnO NW having diameter of 41 nm fabricated by the thermal CVD technique. A high-resolution TEM (HRTEM) image of pure ZnO NW having good crystalline structure is shown in Fig. 5b. It is confirmed from Fig. 5b that the inter-planner distance (d-spacing) between two adjacent lattice planes is approximately 0.26 nm, which resembles (002) planes

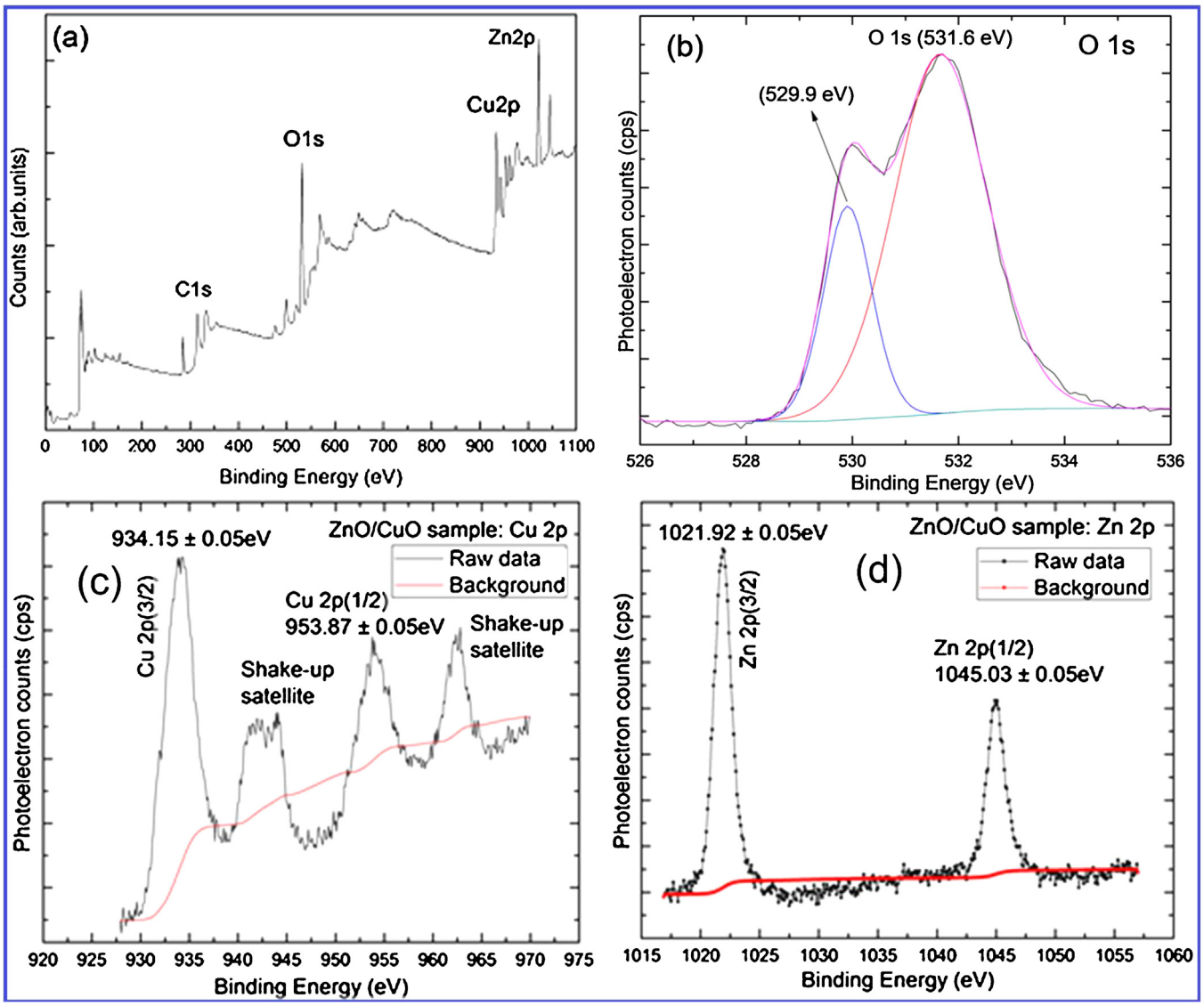


**Fig. 4.** X-ray photoelectron spectroscopy measurement of ZnO/CuO core-shall heterojunction nanowires (a) Profile survey spectra of ZnO/CuO core-shall heterojunction nanowires (b-d) High resolution X-ray photoelectron spectroscopy measurement of O 1s, Cu 2p and Zn 2p, respectively.

in hexagonal wurtzite of pure ZnO structure. The corresponding selected area electron diffraction (SAED) of ZnO NWs is given in Fig. 5c. The dot pattern in SAED shows that the structure of the nanowire has single-crystalline and the d-spacing analysis indicates that the growth is along the [002] direction. Fig. 5d shows a transmission electron microscopy image at the edge of vertically aligned *n*-ZnO/p-CuO core-shell heterojunction NW with p-type CuO nanostructure shells covering n-type ZnO nanowires cores. The diameter of the ZnO/CuO heterostructure nanowire increased about 10 nm compared to pure ZnO NWs. The high-resolution TEM (HRTEM) at the boundary of the *n*-ZnO/p-CuO core-shell heterojunction NW is shown in Fig. 5e, which clearly reveals an interface between the two crystals (core ZnO and CuO shell). The CuO nanostructure shell on the side of ZnO core was shown by the interface marked in the dashed line. The CuO materials are nearly uniformly deposited over the core of nanowires making a thin layer of CuO nanostructure as a shell on the surface of ZnO NW. The thickness of the CuO nanoshell is around 8–10 nm, which is consisted of nanocrystals ranging in size from 3 to 10 nm. As the core material (ZnO) is almost uniformly covered by CuO nanostructure shell, which consists of nanocrystals, we can see that the attached CuO nanocrystals have randomly oriented and crossed-fringe shape on the side (edge) of the core ZnO nanowire. The fringe spacing of nanocrystals corresponds to a CuO (002), (111) and (−202) of lattice spacing of 0.25, 0.23 and 0.19 nm, respectively, of the Monoclinic phase of CuO (JCPD 89–5899). It is also obvious from Fig. 5e of the vertically aligned and large area ZnO/CuO core-shell heterojunction nanowires that the interface between the two crystalline materials is abrupt, which shows that at the interface there is no elemental intermixing. The HRTEM images that clearly show the interface between two crystals are given in Fig. S4 (Supporting Information). The corresponding selected area electron diffraction (SAED) pattern further supports that the nanostructure shells are polycrystalline monoclinic structures of CuO, which is given in Fig. 5f. The successful fabrication of control growth and vertically aligned ZnO/CuO core-shell heterojunction nanowires (NWs) with large area have been developed using a new modified thermal CVD in conjunction with PVD followed by thermal oxidation. One of the key processes in these techniques that have been investigated is the well-controlled growth mechanism, which makes it possible to control crystal structure, surface morphologies and uniform devel-

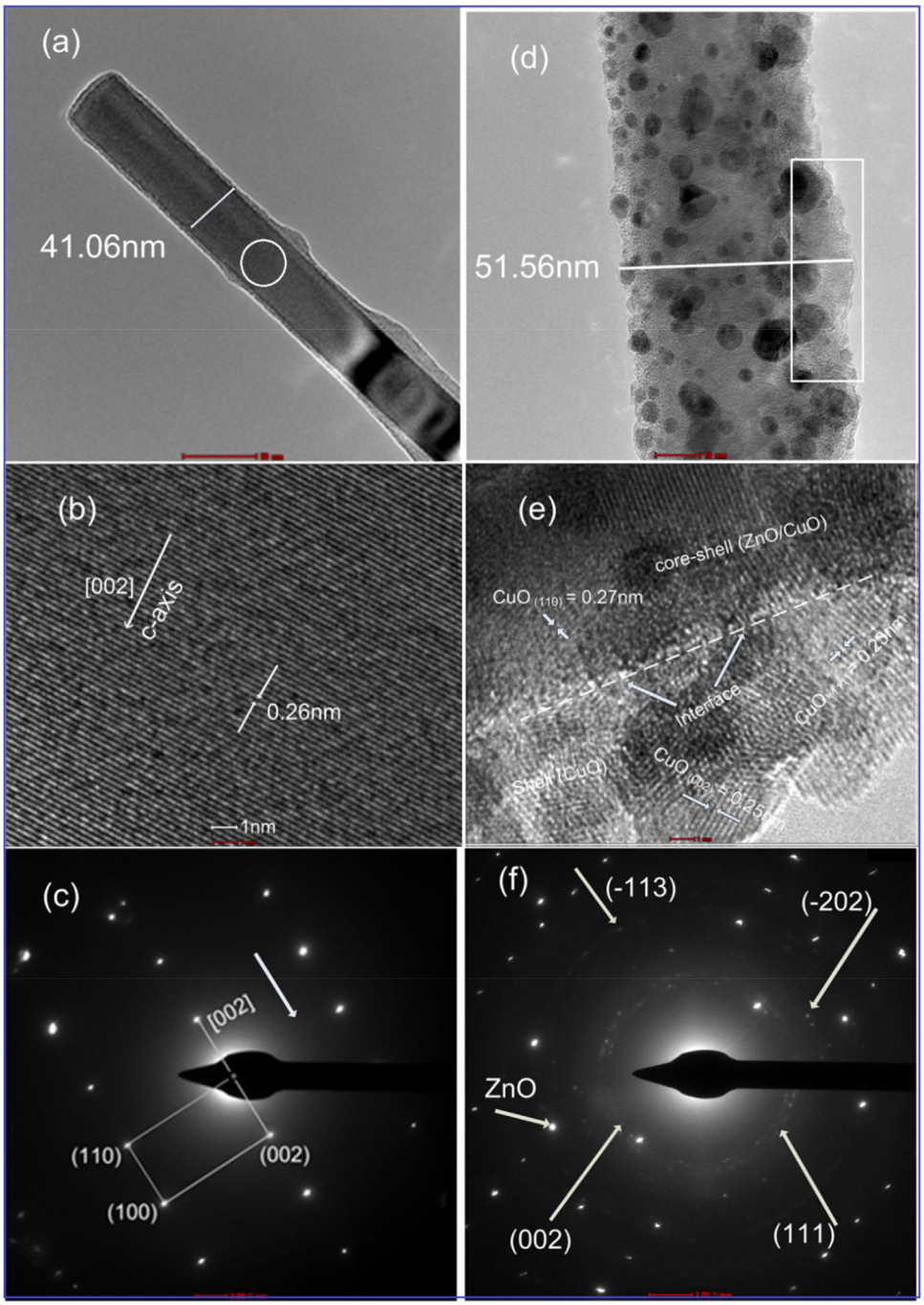


**Fig. 5.** (a) TEM image of single pure ZnO nanowire (b) HRTEM image of pure ZnO NW (c) Pure ZnO NW indicating by SAED pattern showing the growth direction is [002] (d) *n*-ZnO/p-CuO core-shell heterojunction nanowire is shown by TEM image (e) HRTEM image of *n*-ZnO/p-CuO core-shell heterojunction nanowire showing the interface and shell thickness (f) The selected area electron diffraction (SAED) pattern of *n*-ZnO/p-CuO core-shell heterojunction nanowire.

opment of core-shell heterojunction nanowires (NWs) with large area by a catalyst free vapor deposition and oxidation approach.

Fig. 6 shows additional structural information of pure ZnO NW arrays and *n*-ZnO/p-CuO core-shell heterojunction NW arrays obtained by Raman spectroscopy using the measurement range of 50–1100 $cm^{-1}$ at room temperature [25]. In general, ZnO of wurtzite structure has belonged to $C_{6v}{}^{4}$ (P63mc) known as a space group. The space group has six active Raman modes of $E_2(L)$ + $E_2(H)$ + A1T + A1L + E1T + E1L [26,27]. The pure ZnO NWs presented their Raman spectrum peaks at 99, 227, 437, 666 and 939 $cm^{-1}$ [25,28–30]. The Raman spectrum of pure ZnO NWs is shown in Fig. 6. The peaks at 99 and 437 $cm^{-1}$ are referred to as $E_2(L)$ and $E_2(H)$ Raman modes of pure ZnO nanowire, respectively [30,31], whereas the peaks at 227, 666 and 939 $cm^{-1}$ are referred to as 2TA, [TA+ LO] and 2TO modes, respectively. In comparison of vertical aligned ZnO NWs, the Raman spectrum of the vertically aligned ZnO/CuO core-shall heterojunction NW arrays shows three new peaks at 302, 346 and 625 $cm^{-1}$, which can be referred to as Ag, $Bg_1$, and $Bg_2$ modes, respectively. These modes are consistent with the previous report on CuO crystal and literature [32–37]. The presence of ZnO and CuO Raman modes further reveals that the Raman spectroscopy measurements analysis supports the core-shell heterojunction nanowires, which is in agreement with the XRD and TEM results.

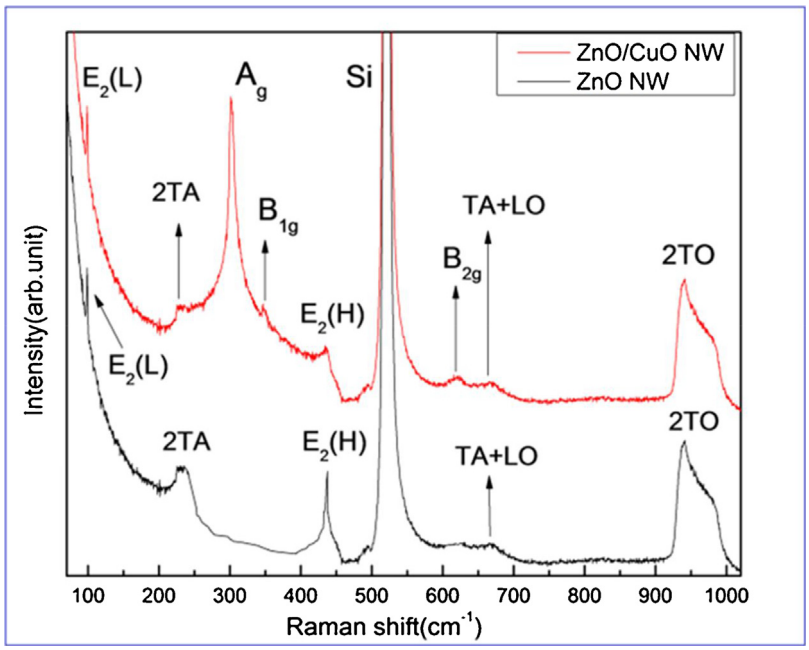


**Fig. 6.** Raman spectroscopy measurements analysis for pure ZnO NWs and ZnO/CuO core-shell heterojunction NW arrays.

The microstructure and composition of the core-shell nanowires were further investigated by energy dispersive X-ray (EDX) spectrum and EDX elemental mappings as shown in Fig. 7. To avoid any interference with ZnO/CuO core-shall heterojunction NW, the TEM grid of Ni is used as a representative to support the individual nanowire sample. The EDX spectrum measured from a single nanowire is shown in Fig. 7a. The EDX spectrum measured from tip, middle and bottom of the nanowires showing their elemental analysis is shown in Fig. 7(b, c, d). EDX spectrum analysis revealed that 53.64 wt.% of Cu has been added to the top surface of the ZnO nanowire tip portion, 52.25 wt.% of copper (Cu) has been added to the middle portion of the ZnO nanowire surface and 48.82 wt.% of Cu has been added to the bottom part of the core-shell nanowire. The significant amount of copper deposition on three different places (tip, middle and bottom) of a single nanowire shows very little difference, which indicates that Cu is nearly uniformly deposited on the vertical aligned ZnO NWs. The significant amount of copper deposition provides further evidence of the thin shell formation on vertically aligned ZnO NWs. Furthermore, Fig. 7(e–h) shows the electron scan image of single core-shell NW and their EDX elemental mappings of oxygen (O), copper (Cu), and zinc (Zn), respectively. Fig. 7(f–h) reveals that the core-shell NW heterostructure is consisted only of elements of copper, zinc and oxygen, while their EDX elemental mapping shows the uniform distribution of core and shell materials. From the EDX elemental analysis and mapping, we further suggest that CuO nanoshell is grown nearly uniformly as an epitaxial layer onto core ZnO, resulting in a large area of vertically aligned *n*-ZnO/p-CuO core-shell heterojunction nanowires. The well-known analysis of EDX and elemental mapping observations indicate that the thermal CVD grown ZnO nanowires followed by Cu sputtering and its thermal oxidation have successfully produced a large area of vertically well-aligned ZnO/CuO core-shell nanowire arrays.

### 3.4. Optical study

#### 3.4.1. Photoluminescence

Fig. 8 shows the room-temperature PL spectra of ZnO NWs and ZnO/CuO core-shell heterojunction nanowires. The inset has shown magnified spectra of ZnO NWs and ZnO/CuO core-shell heterojunction nanowires. The PL spectrum of ZnO NWs exhibits two emissions, a UV emission band of ZnO NWs centered at 378 nm originates from the exciton recombination radiation [38]. The visible emission band at 751 nm is due to the recombination radiation of electrons in a deep defect level or a shallow surface defect level with holes in a valence band [39]. Compared to bare ZnO NWs, ZnO/CuO core-shell heterojunction nanowires peak shifted in UV region from 374 nm to 384 nm, while the peaks, which is due to the recombination radiation of electrons in a deep defect level or a shallow surface defect level with holes in a valence band, shifted from 751 nm to 770 nm. Also, the intensity ratio of the UV peak and the visible light peak of ZnO/CuO NWs would increase [40]. This may be because CuO covers the surface of ZnO NWs, reducing the surface defects of ZnO NWs, corresponding to the decreases in energy band and in enhanced UV peak and visible peak. The shifting of the UV peak and the visible light peak to the shorter wavelength of ZnO/CuO NWs is due to the surface modification as compared to ZnO NWs. Core ZnO NWs covered by CuO nanostructure shell can lead to hinder the observation of the visible emission, which is usually observed from ZnO (green band emission of ZnO). The energy band of ZnO/CuO core-shell heterojunction NWs decreases due to the shifting of the UV peak and the visible light peak to the shorter wavelength as compared to bare ZnO NWs. Hence the enhancement of intensity ratio and decreasing the energy band by ZnO/CuO core-shell heterojunction NWs may be very useful in photocatalysts and in solar energy conversion applications [40].

#### 3.4.2. UV–vis reflectance spectroscopy

The optical property of the ZnO NWs and their core-shell (*n*-ZnO/p-CuO) heterojunction NWs has been also analyzed for the prepared samples at room temperature by using UV–vis reflectance spectroscopy. For accurate and precise determination of the reflectance spectra, we studied the reflection efficiency of the as fabricated ZnO NWs and vertically aligned *n*-ZnO/p-CuO core-shell heterojunction nanowires grown on silicon substrates using bare silicon as a reference substrate. The UV–vis specular reflection spectra of the synthesized ZnO nanowires and their vertical aligned ZnO/CuO core-shell heterojunction nanowires developed

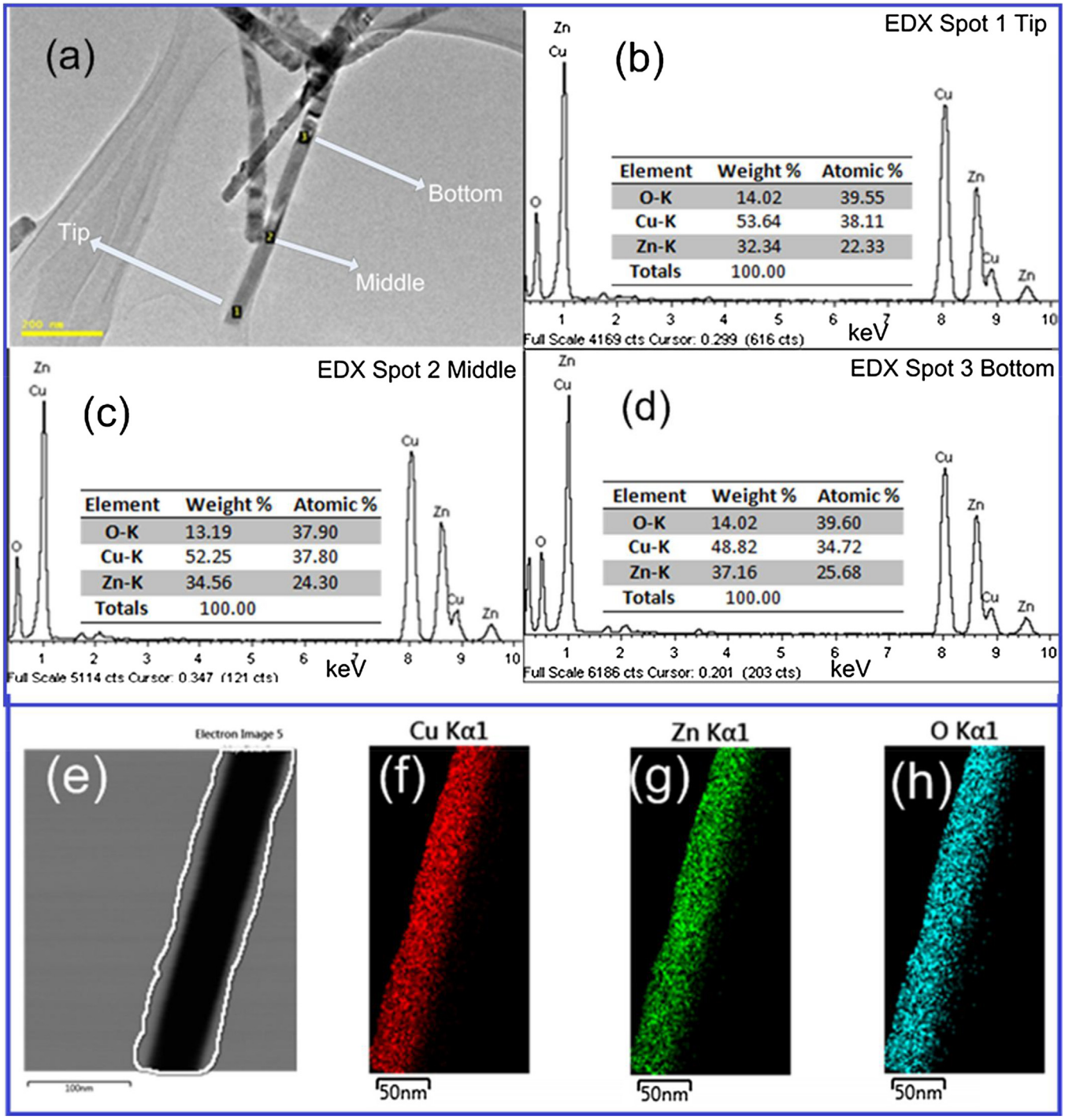


**Fig. 7.** EDX spectrum measured from single ZnO/CuO core-shell nanowire (a) tip (b) middle, (c) and bottom showing their elemental analysis. Figure (e) shows the single core-shell NW image and Figure (f), (g) and (h) shows their EDX elemental mappings of Cu, Zn and O, respectively.

on Si substrates are given in Fig. 9. The reflectance spectra of the vertical aligned ZnO/CuO core-shell heterojunction nanowires were studied for sputter copper deposition time of 3 min and 4 min on vertical aligned ZnO nanowires. The reflectance spectra of pure ZnO showed a sharp increase at 378 nm and the material had a strong reflective characteristic after approximately 420 nm. The as synthesized ZnO nanowire arrays show a maximum reflectance of approximately 42% in the 200–800 nm range. The reflectance of ZnO/CuO core-shell heterojunction NW arrays, for which copper sputter deposition time is 3 min, decreases to 29%, while for copper sputter with deposition time of 4 min, the reflectance spectra of core-shell (ZnO/CuO) heterojunction nanowires decreases to 24%. The reflectance can be explained on the basis of modification in the structural characteristics (diameter of the NWs, surface roughness, etc.) of the ZnO/CuO core-shell heterojunction NW array for different sputtering deposition time on vertically aligned ZnO nanowire arrays. The reflectance efficiency in the visible spectrum decreased with increasing copper sputter deposition time followed by thermal oxidation. This means that by loading of CuO onto the vertical align ZnO NW arrays, the reflectance efficiency of core-shell heterojunction NWs decreases, while absorption efficiency increases. However, there was no apparent difference in the absorption edge

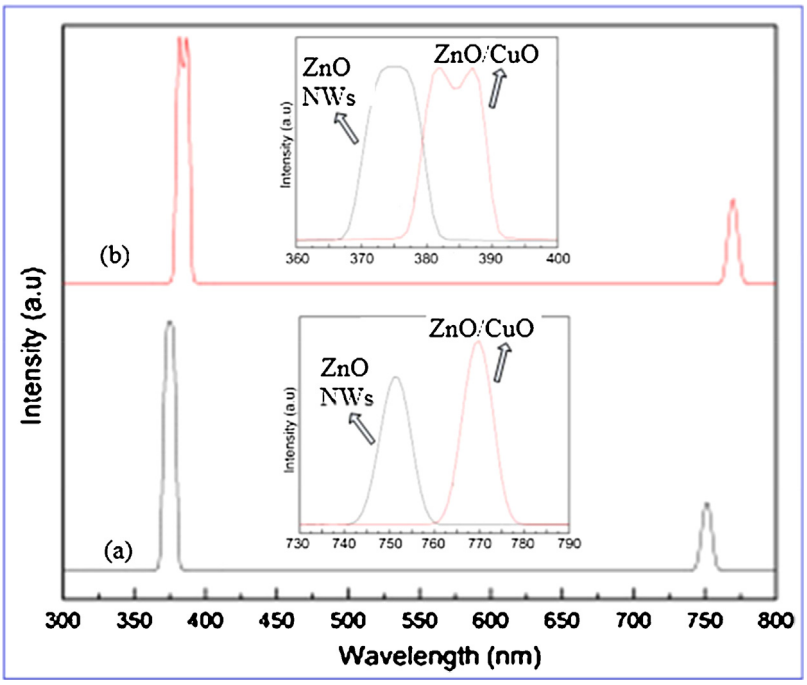


**Fig. 8.** Room temperature PL spectrum measured from (a) ZnO NWs and (b) the fabricated *p*-CuO/n-ZnO heterojunction nanostructure.

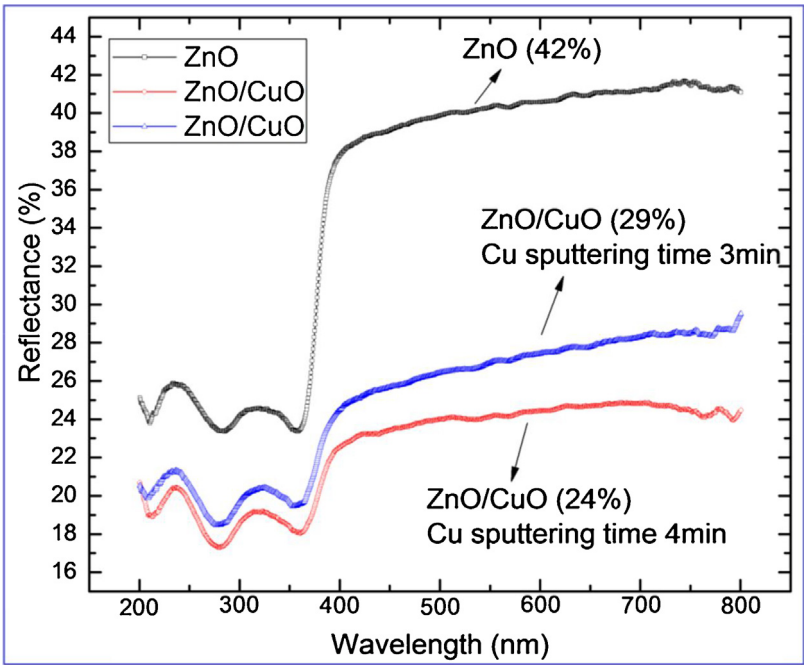


**Fig. 9.** UV–vis reflectance spectra of ZnO and ZnO/CuO core-shell heterojunction NWs.

between the pure ZnO NWs and ZnO/CuO core-shell heterojunction NWs. This provides evidence that CuO was deposited on the ZnO surface rather than integrated into the ZnO lattice location. It has been noted that ZnO having band gap 3.37 eV has quite low reflectance efficiency in the UV region (200–380 nm), while it has better absorption efficiency in the UV region (200–380 nm). From Fig. 9, one can see that pure ZnO nanowire arrays showed quite low reflectance values in the UV region (200–380 nm), which indicates a very high absorption in this region, and the reflectance rises in the visible region (400–750 nm). It has been reported that CuO with a direct band gap of 1.2 eV has a low reflectance peak in the range of 300 nm to 600 nm. Therefore, in comparison to pure ZnO nanowires, the vertically aligned ZnO/CuO core-shell heterojunction nanowire arrays definitely showed lower reflectance value or high absorption value in the visible region (400–750 nm). From the result of optical analysis, it is clear that the synthesized core-shell heterojunction nanowires possessed advanced light absorption ability in the visible region, which is about 18% more absorption as compared to pristine ZnO nanowires. The suppressing surface recombination and enhanced UV–vis absorption of ZnO/CuO core-shell heterojunction nanowires can greatly improve the performance of nanodevices [19]. The ability of advanced light

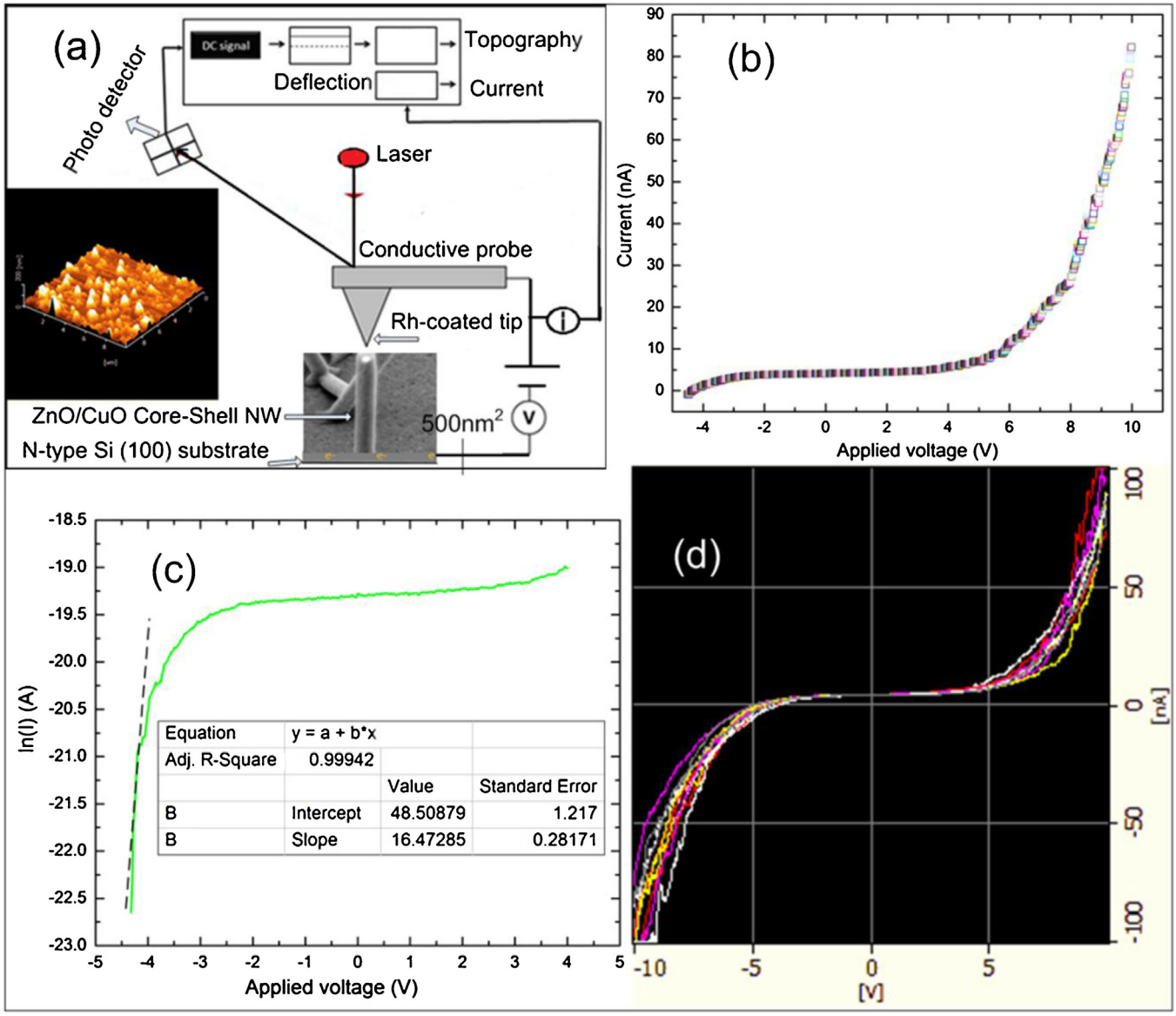


**Fig. 10.** Current-voltage characteristics of the vertically aligned ZnO/CuO core-shall heterojunction nanowires at atmospheric room temperature (a) Schematic of the C-AFM for current-voltage measurement, the inset is the AFM image of core-shell heterojunction nanowires (b) The *I–V* measurement of the nanodiode at the interface of the core-shell heterojunction nanowires (c) Semi-log *I –V* measurement of the core-shell heterojunction nanowires (d) The *I-V* characteristics curves recorded from the center of the core-shell heterojunction nanowires at different points using Conductive-AFM in contact mode..

absorption in core-shell heterojunction nanowires leads to the application in advanced photovoltaic and solar energy conversion devices. It is expected that the present ZnO/CuO core-shell heterojunction nanowire devices could find potential applications in future high-performance optoelectronic devices, particularly solar cells, field emitters, and sensor devices.

### 3.5. *Electrical measurement* (I–V *characteristic)*

To measure the *I–V* characteristic and rectifying behavior of *n*-ZnO/p-CuO core-shell heterojunction NWs about the junction development at interface, electrical measurements were studied by conductive AFM. To contact the NWs fabricated on an n-type silicon substrate, the conductive AFM (C-AFM) used the conductive tip as a movable electrode in contact mode at atmospheric room temperature. Fig. 10a shows the schematic of the C-AFM for current-voltage measurement. In the inset in Fig. 10a is shown the AFM image of core-shell heterojunction nanowire arrays. Fig. 10b represents the *I–V* characteristic properties of the p-n junction at the interface of *n*-ZnO/p-CuO core-shell heterojunction nanowires, where the measurement was observed from −10 V to +10 V of the applied voltage. The *I–V* characteristic curve of the core-shell heterojunction nanowires reveals good rectifying nature and the rectification ratio for $I_F/I_R$ is about $I_{+4.3}/I_{-4.3} = 5.7 \times 10^1$ at 4.3 V. The good rectifying behavior and rectification ratio about the p-n junction formation indicates the formation of a nanoscale-diode. The turn on or cut-in voltage to conduct the current in the forward direction of the core-shell heterostructure nanowires at the interface of p-n junction is about 2.5 V, whereas the leakage current of reverse bias at the interface of p-n junction is about 0.104 nA under 4.3 V reverse bias, respectively. The heterojunction shows a very small amount of leakage current of reverse bias, which perhaps is due to the low level interface defect recombination at the interface of both materials having core ZnO and shell CuO materials [28,41]. Additionally from a semi-log representation of the *I–V* characteristics of Fig. 10c, the nanodiode ideality factor was measured using standard diode

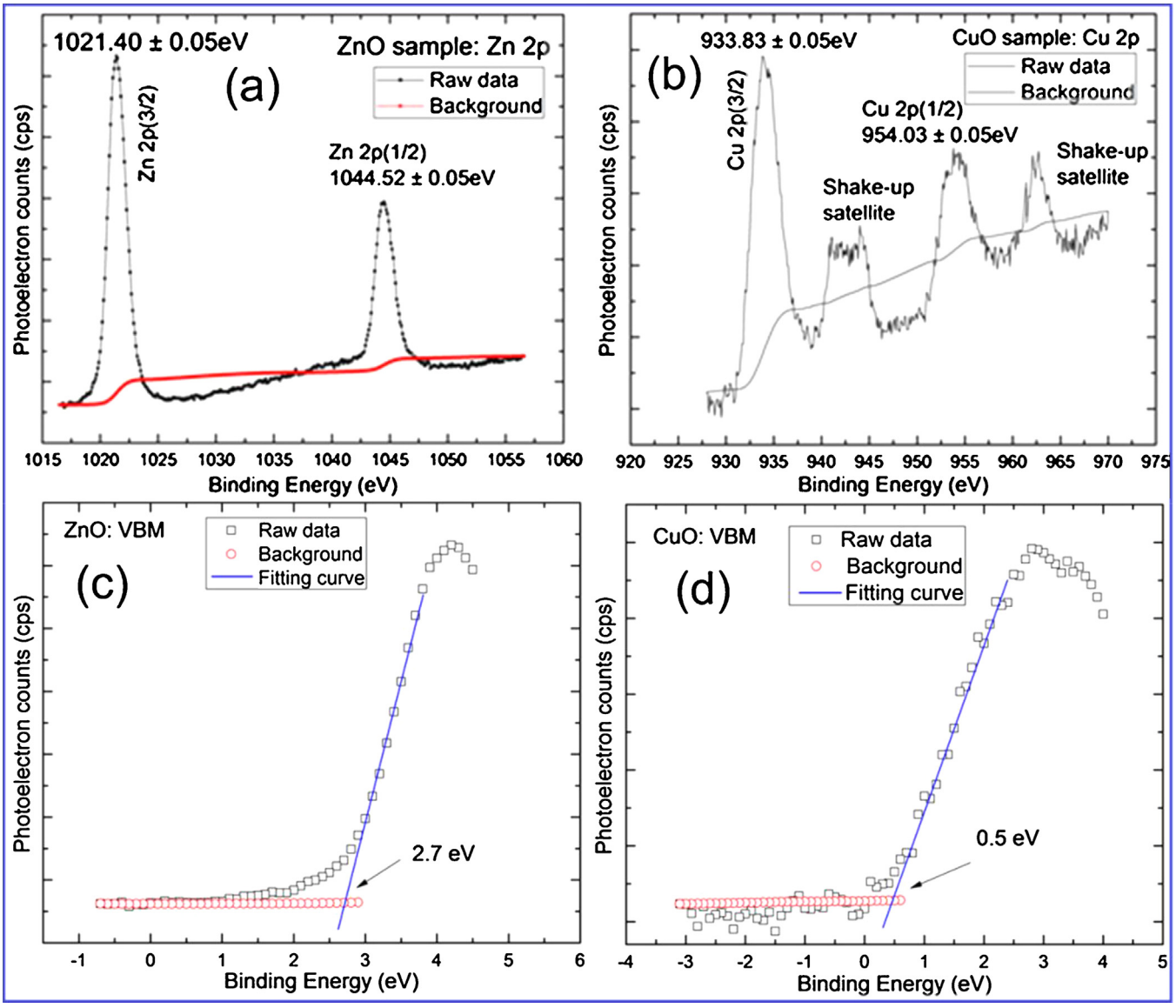


**Fig. 11.** XPS core-level (CL) and Valence-band edge (VBE) spectra (a) CL of Zn $2p_{3/2}$ for ZnO (b) CL of Cu $2p_{3/2}$ for CuO (c) VBE spectra for ZnO (d) VBE spectra for CuO.

equation and was found to be 2.3 from a semi-log *I–V* curve using the slope of the linear region. Fig. 10d has shown the excellent *I–V* characteristics curves of nano-diode recorded from the center of core-shell heterojunction nanowires using the conductive-AFM in contact mode. For the vertically aligned ZnO/CuO core-shell heterojunction nanowires, the current follows the standard diode equation and it increases exponentially. The exponential increase of the current is usually noticed in wide band gap of p-n junction diodes as a result of recombination tunneling mechanism [42]. As compared to ideal value, the variation of the ideality factor is possibly due to the structural defects, barrier tunneling or changes in the interface composition [43–45].

The good rectification value and close relation to the ideality factor indicates that our *I–V* characteristic of the core-shell heterojunction nanowires developed by catalyst free vapor deposition and oxidation approach is quite good. This study and results presented here indicate the applicability of ZnO/CuO core-shell heterojunction nanowires for the fabrication of efficient and low-cost optoelectronic nanostructure devices such as photodetectors, field emitters, solar cells, and sensor devices.

### 3.6. Band offset measurements at ZnO/CuO heterointerfaces

Accurate band offset (BOs) measurement at the interfaces of core-shell heterojunction nanowires play an important role in the application of semiconductor devices and to perceive the significance relationship between the physical structure of heterointerfaces, carrier transport and electronic structure [46–52]. XPS is the direct and dominant technique for the measurement of valance band discontinuities/offsets at ZnO/CuO heterointerfaces [53]. To find the Valance band offset of ZnO/CuO core-shell heterojunction nanowires, the high-resolution spectra of the synthesized samples of ZnO, CuO and ZnO/CuO heterojunction nanowires were found and tabulated in Table 1. The Valence band offset (VBO) value at ZnO/CuO heterointerfaces can be measured by Kraut et al. formulation [54,55], which is given in Eq. (1).

$$\Delta E_V = \Delta E_{CL} - \left[\left(E^{ZnO}_{Zn\,2p(3/2)} - E^{ZnO}_{VBM}\right) - \left(E^{CuO}_{Cu2p(3/2)} - E^{CuO}_{VBM}\right)\right] \quad (1)$$

where $\Delta E_{CL} = E^{ZnO/CuO}_{Zn\,2p(3/2)} - E^{ZnO/CuO}_{Cu\,2p(3/2)}$ is the difference of the binding energy between Zn2p and Cu2p core-level (CLs) spectra

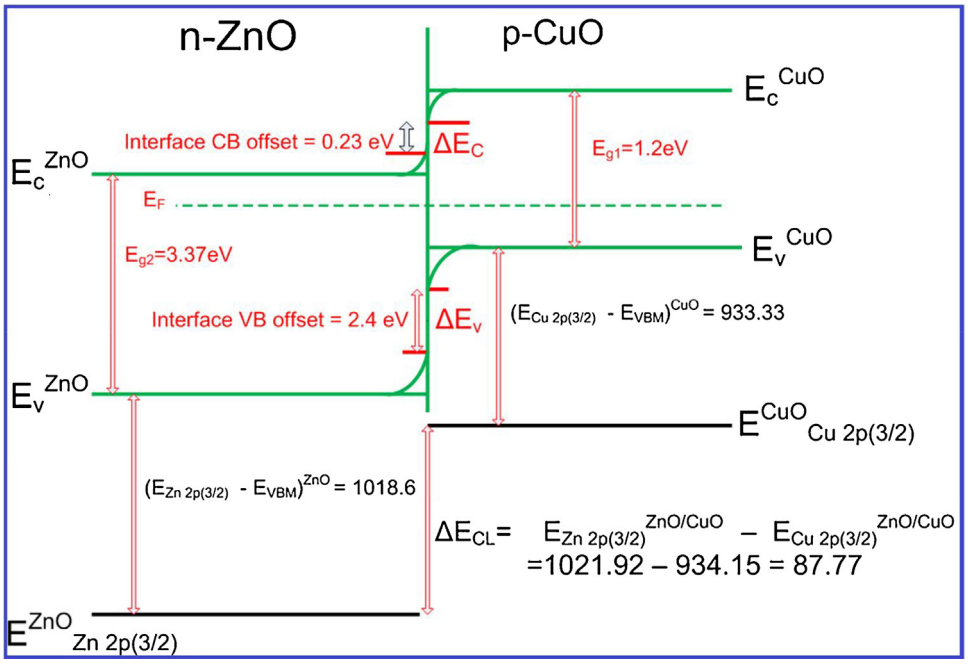


**Fig. 12.** Schematic energy band diagram of type-II band alignment of *p*-CuO/n-ZnO heterojunction.

measured in ZnO/CuO heterojunction, while $\left(E^{ZnO}_{Zn\,2p(3/2)} - E^{ZnO}_{VBM}\right)$ and $\left(E^{CuO}_{Cu2p(3/2)} - E^{CuO}_{VBM}\right)$ are the binding energies of valance band maximum (VBM) with respect to the core-level positions of samples ZnO and CuO, respectively. The core-level XPS spectra of ZnO/CuO core-shell heterojunction nanowires are shown in Fig. 4(c, d), whereas the CL and valance band spectra of ZnO and CuO samples are given in Fig. 11. All the core level binding energy spectra were used for fitting using a Voigt (mixed Lorentz–Gaussian), which is a line shape, and Shirley background was used for the calculation. The positions of valance band maximum (VBM) are determined by extrapolating using a linear fit to the leading edge of the valance band spectra to the background level in order to examine the finite settlement of the spectrometer [48]. All the spectra and their binding energy obtained from the core-level (Fig. 4(c, d)) and fitting process (Fig. 11) are given in Table 1.

**Table 1**
Binding energies obtained from the core-level and fitting process for the synthesized samples.

| Sample | Region (core-level) | Binding Energy (eV) |
|---|---|---|
| **n-ZnO** | Zn $2p_{3/2}$ | $1021.40 \pm 0.05$ |
| | VBM | $2.7 \pm 0.05$ |
| **p-CuO** | Cu $2p_{3/2}$ | $933.83 \pm 0.05$ |
| | VBM | $0.5 \pm 0.05$ |
| **ZnO/CuO** | Zn $2p_{3/2}$ | $1021.92 \pm 0.05$ |
| | Cu $2p_{3/2}$ | $934.15 \pm 0.05$ |

Table 1 shows synthesized samples and their binding energies for the core-level peak position and their valance band maximum position. The measured value for the valance band offsets (VBO) using Eq. (1), i.e. $\Delta E_V$ (VBO) at ZnO/CuO heterointerface, is found to be 2.4 eV. In addition, *Hussian* et al. measured the VBO value of the composite heterostructure of ZnO/CuO heterojunction, which is found to be 2.83 eV by XPS using hydrothermal technique [56] and is bigger than our current result. This aspect may be due to the different growth process of one dimensional ZnO/CuO heterostructure nanowires, which cause a different atomic adjustment at ZnO/CuO interface. The conduction-band offset (CBO) of ZnO/CuO heterojunction nanowires is given by Eq. (2).

$$\Delta E_C = E_g^{ZnO} - E_g^{CuO} - \Delta E_V \quad (2)$$

The band gaps of ZnO and CuO at room temperature are ($E_g^{ZnO} = 3.37\,eV$ [57] and $E_g^{CuO} = 1.2\,eV$ [58]), respectively. So by substituting these values and $\Delta E_V = 2.4$ eV, the CBO is estimated to be 0.23 eV. The schematic energy band diagram is deduced based on the aforementioned analysis as shown in Fig. 11. We can examine that a type-II band alignment structure is found at ZnO/CuO interface. The measured VBO ($\Delta E_V$) is greater than the conduction band offset ($\Delta E_C$) as shown in Fig. 12. The large $\Delta E_V$ of core-shell heterojunction at the interface should result in a thin tunneling barrier across the p-n junction [59]. In addition, the result in large value of $\Delta E_V$ is important due to carrier confinement for device applications like heterostructure field effect transistors or light emitters [49]. The relatively large valance band offset (VBO) value extracted here would also contribute to suppressing light radiation in the visible part as it reduces the transport of holes from the CuO to ZnO [56]. We suggest that the result of this study contributes to further improvements in solar energy conversion and advanced nano-optoelectronic devices.

## 4. Conclusions

In conclusion, vertically aligned ZnO/CuO core-shell heterojunction nanowires (NWs) with large area have been successfully fabricated on a silicon substrate without using any catalyst or seed layer by combining the thermal CVD and physical vapor deposition (PVD) techniques. Morphological and structural investigation has shown that the core ZnO NWs were grown perpendicularly and uniformly having diameter in the range of 35–45 nm and length of about 700–1300 nm, respectively, while the CuO nanostructure shell with a thickness of $8 \sim 10$ nm were grown epitaxially onto the core ZnO nanowires. The optical property analysis has revealed that the synthesized core-shell heterojunction nanowires possessed advanced light absorption ability in the visible region, which is about 18% more absorption as compared to pristine ZnO nanowires. The electrical measurements with a conducting tip AFM confirmed

the excellent rectifying behavior with rectification ratio ~57 and ideality factor was found to be 2.3, originating from the 1D coaxial p-n junction diode developed at the interface of core-shell heterojunction nanowires. The accurate band offsets (BOs) at ZnO/CuO heterointerfaces have been measured by X-ray photoelectron spectroscopy (XPS) and a type-II band alignment structure were found at ZnO/CuO interface. The result of this study has contributed to the advanced device heterostructures like p-n junctions, which is the base of functional nanodevices for the development of new nanostructured phase and is favorable for solar energy conversion and optoelectronic applications.

## Acknowledgments

This research work was supported by the Malaysian Ministry of Higher Education (MOHE) through the Research Management Centre (RMC), Universiti Teknologi Malaysia research grant "LRGS vote no. 4L825" under Research Alliance in Frontier Materials. The authors gratefully acknowledge the Higher Education Commission (HEC) Pakistan for the financial support to Muhammad Arif Khan through Partial Support for Ph.D. Studies Abroad grant No: 1-8/HEC/HRD/2015/5050 (k).

## Appendix A. Supplementary data

Supplementary data associated with this article can be found, in the online version, at https://doi.org/10.1016/j.apsusc.2017.11.071.

## References

[1] K.C. Pradel, Y. Ding, W. Wu, Y. Bando, N. Fukata, Z.L. Wang, Optoelectronic properties of solution grown ZnO n – p or p – n core-shell nanowire arrays, ACS Appl. Mater. Interfaces 8 (2016) 4287–4291.
[2] K.I. Hunter, J.T. Held, K.A. Mkhoyan, U.R. Kortshagen, Nonthermal plasma synthesis of Core/Shell quantum dots: strained Ge/Si nanocrystals, ACS Appl. Mater. Interfaces (2017) 16170.
[3] M. Sakurai, Y.G. Wang, T. Uemura, M. Aono, L. Xu, X. Li, et al., Coaxial silicon nanowires as solar cells and nanoelectronic power sources, Nanotechnology 7 (2015) 20264–20271.
[4] Y. Tak, S.J. Hong, J.S. Lee, K. Yong, Solution – based synthesis of a CdS Nanoparticle/ZnO nanowire heterostructure array, Cryst. Growth Des. 9 (2009) 2627–2632.
[5] K.M. Mcpeak, J.B. Baxter, ZnO nanowires grown by chemical bath deposition in a continuous flow microreactor, Cryst. Growth Des. 9 (2009) 4538–4545, http://dx.doi.org/10.1021/cg900551f.
[6] S. Dhara, P.K. Giri, ZnO nanowire heterostructures: intriguing photophysics and emerging applications, Rev. Nanosci. Nanotechnol. 2 (2013) 147–170, http://dx.doi.org/10.1166/rnn.2013.1032.
[7] P. Zhu, Z. Weng, X. Li, X. Liu, S. Wu, K.W.K. Yeung, et al., Biomedical applications of functionalized ZnO nanomaterials: from biosensors to bioimaging, Adv. Mater. Interfaces 3 (2015) 1500494, http://dx.doi.org/10.1002/admi.201500494.
[8] Z. Zang, X. Tang, Enhanced fluorescence imaging performance of hydrophobic colloidal ZnO nanoparticles by a facile method, J. Alloys Compd. 619 (2015) 98–101, http://dx.doi.org/10.1016/j.jallcom.2014.09.072.
[9] Z. Zang, X. Zeng, J. Du, Ming Wang, X. Tang, Femtosecond laser direct writing of microholes on roughened ZnO for output power enhancement of InGaN light-emitting diodes, Opt. Lett. 41 (2016) 3463–3466.
[10] Y. Chen, Q. Jia, Z. Shen, J. Zhao, Z. Zhao, H. Ji, et al., A cuO-ZnO nanostructured p-n junction sensor for enhanced n-butanol detection, RSC Adv. 6 (2016) 2504–2511.
[11] S. Dhara, K. Imakita, P.K. Giri, M. Mizuhata, M. Fujii, Aluminum doped core-shell ZnO/ZnS nanowires: doping and shell layer induced modification on structural and photoluminescence properties, J. Appl. Phys. 114 (2013) 1–8, http://dx.doi.org/10.1063/1.4824288.
[12] S.S. Wilson, Y. Tolstova, D.O. Scanlon, G.W. Watson, H.A. Atwater, Interface stoichiometry control to improve device voltage and modify band alignment in ZnO/Cu2O heterojunction solar cells, Energy Environ. Sci. 7 (2014) 3606–3610, http://dx.doi.org/10.1039/C4EE01956C.
[13] A. Kargar, Y. Jing, S.J. Kim, C.T. Riley, X. Pan, D. Wang, ZnO/CuO heterojunction branched nanowires for photoelectrochemical hydrogen generation, ACS Nano 7 (2013) 11112–11120, http://dx.doi.org/10.1021/nn404838n.
[14] N.O.V. Plank, H.J. Snaith, C. Ducati, J.S. Bendall, L. Schmidt-Mende, M.E. Welland, A simple low temperature synthesis route for ZnO-MgO core-shell nanowires, Nanotechnology 19 (2008) 465603, http://dx.doi.org/10.1088/0957-4484/19/46/465603.
[15] G. Filipič, U. Cvelbar, Copper oxide nanowires: a review of growth, Nanotechnology 23 (2012) 194001, http://dx.doi.org/10.1088/0957-4484/23/19/194001.
[16] J. Kim, W. Kim, K. Yong, CuO/ZnO heterostructured nanorods: photochemical synthesis and the mechanism of H2S gas sensing, J. Phys. Chem. C 116 (2012) 15682–15691, http://dx.doi.org/10.1021/jp302129j.
[17] C.H. Xu, C.H. Woo, S.Q. Shi, The effects of oxidative environments on the synthesis of CuO nanowires on Cu substrates, Superlatt. Microstruct. 36 (2004) 31–38, http://dx.doi.org/10.1016/j.spmi.2004.08.021.
[18] S. López-Romero, M. García-H, Photoluminescence and structural properties of ZnO nanorods growth by assisted-hydrothermal method, World J. Condens. Matter Phys. 3 (2013) 152–157, http://dx.doi.org/10.4236/wjcmp.2013.33024.
[19] P.Y. Michael, H. Huang, Yiying Wu, Henning Feick, Ngan Tran, Eicke Weber, Catalytic growth of zinc oxide nanowires, Adv. Mater. 13 (2001) 113–116, http://dx.doi.org/10.1002/1521-4095(200101)13:2<113::AID-ADMA113>3.0.CO;2-H.
[20] U.N. Maiti, S. Maiti, S. Goswami, D. Sarkar, K.K. Chattopadhyay, Room temperature deposition of ultra sharp ZnO nanospike arrays on metallic, non-metallic and flexible carbon fabrics: efficient field emitters, CrystEngComm 13 (2011) 1976, http://dx.doi.org/10.1039/c0ce00618a.
[21] S. Anandan, G.J. Lee, J.J. Wu, Sonochemical synthesis of CuO nanostructures with different morphology, Ultrason. Sonochem. 19 (2012) 682–686, http://dx.doi.org/10.1016/j.ultsonch.2011.08.009.
[22] K.K.C.C.K. Ghosh, S.R. Popuri, T.U. Mahesh, Preparation of nanocrystalline CuAlO2 through sol–gel route, J. Sol-Gel Sci. Technol. 52 (2009) 75–81, http://dx.doi.org/10.1007/s10971-009-1999-x.
[23] C. Furlani, G. Mattogno, F.M. Capece, V. Di Castro, Copper chrcmite catalysts: XPS structure and correlation with catalytic activity, J. Electron Spectros. Relat. Phenomena 27 (1982) 119–128.
[24] A.A. Ashkarran, S.A.A. Afshar, S.M. Aghigh, M. Kavianipour, Photocatalytic activity of ZnO nanoparticles prepared by electrical arc discharge method in water, Polyhedron 29 (2010) 1370–1374, http://dx.doi.org/10.1016/j.poly.2010.01.003.
[25] J.X. Wang, X.W. Sun, Y. Yang, K.K. a Kyaw, X.Y. Huang, J.Z. Yin, et al., Free-standing ZnO-CuO composite nanowire array films and their gas sensing properties, Nanotechnology 22 (2011) 325704, http://dx.doi.org/10.1088/0957-4484/22/32/325704.
[26] F.J. Manjon, B. Mari, J. Serrano, A.H. Romero, Silent Raman modes in zinc oxide and related nitrides, J. Appl. Phys. 97 (2005) 1–4, http://dx.doi.org/10.1063/1.1856222.
[27] N. Ashkenov, B.N. Mbenkum, C. Bundesmann, V. Riede, M. Lorenz, D. Spemann, et al., Infrared dielectric functions and phonon modes of high-quality ZnO films, J. Appl. Phys. 93 (2003) 126, http://dx.doi.org/10.1063/1.1526935.
[28] S. Pal, S. Maiti, U.N. Maiti, K.K. Chattopadhyay, Low temperature solution processed ZnO/CuO heterojunction photocatalyst for visible light induced photo-degradation of organic pollutants, CrystEngComm 17 (2015) 1464–1476, http://dx.doi.org/10.1039/C4CE02159B.
[29] H. Zhu, J. Iqbal, H. Xu, D. Yu, Raman and photoluminescence properties of highly Cu doped ZnO nanowires fabricated by vapor-liquid-solid process, J. Chem. Phys. 129 (2008) 1–5, http://dx.doi.org/10.1063/1.2981050.
[30] M. Willander, L.L. Yang, A. Wadeasa, S.U. Ali, M.H. Asif, Q.X. Zhao, et al., Zinc oxide nanowires: controlled low temperature growth and some electrochemical and optical nano-devices, J. Mater. Chem. 19 (2009) 1006, http://dx.doi.org/10.1039/b816619f.
[31] R.S. Sreedharan, V. Ganesan, C.P. Sudarsanakumar, K. Bhavsar, R. Prabhu, V.P.P. Mahadevan Pillai, Highly textured and transparent RF sputtered Eu2O3 doped ZnO films, Nano Rev. 6 (2015) 1–16, http://dx.doi.org/10.3402/nano.v6.26759.
[32] T. Yu, X. Zhao, Z.X. Shen, Y.H. Wu, W.H. Su, Investigation of individual CuO nanorods by polarized micro-Raman scattering, J. Cryst. Growth 268 (2004) 590–595, http://dx.doi.org/10.1016/j.jcrysgro.2004.04.097.
[33] J.F. Xu, W. Ji, Z.X. Shen, W.S. Li, S.H. Tang, X.R. Ye, et al., Raman spectra of CuO nanocrystals, J. Raman Spectrosc. 30 (1999) 413–415, http://dx.doi.org/10.1002/(SICI)1097-4555(199905)30:5<413:AID-JRS387>3.0.CO;2-N.
[34] A. Fallis, Raman scattering from cupric oxide, J. Chem. Inf. Model. 53 (2013) 1689–1699, http://dx.doi.org/10.1017/CBO9781107415324.004.
[35] D.P. Volanti, M.O. Orlandi, J. Andres, E. Longo, Efficient microwave-assisted hydrothermal synthesis of CuO sea urchin-like architectures via a mesoscale self-assembly, CrystEngComm 12 (2010) 1696–1699, http://dx.doi.org/10.1039/B922978G.
[36] S.B. Wang, C.H. Hsiao, S.J. Chang, Z.Y. Jiao, S.J. Young, S.C. Hung, et al., ZnO branched nanowires and the p-CuO/n-ZnO heterojunction nanostructured photodetector, IEEE Trans. Nanotechnol. 12 (2013) 263–269, http://dx.doi.org/10.1109/TNANO.2013.2243916.
[37] S. Fuentes, R.A. Zárate, P. Muñoz, D.E. Díaz-Droguett, Formation of hierarchical cuo nanowires on a copper surface via a room-temperature solution-immersion process, J. Chil. Chem. Soc. 55 (2010) 147–149, http://dx.doi.org/10.4067/S0717-97072010000100034.
[38] Y. Zhang, M.K. Ram, E.K. Stefanakos, D.Y. Goswami, Synthesis, characterization, and applications of ZnO nanowires, J. Nanomater. 2012 (2012) 1–22, http://dx.doi.org/10.1155/2012/624520.
[39] A. Wei, L. Xiong, L. Sun, Y.-J. Liu, W.-W. Li, CuO nanoparticle modified ZnO nanorods with improved photocatalytic activity, Chinese Phys. Lett. 30 (2013) 46202, http://dx.doi.org/10.1088/0256-307X/30/4/046202.

[40] S. Jung, S. Jeon, K. Yong, Fabrication and characterization of flower-like CuO-ZnO heterostructure nanowire arrays by photochemical deposition, Nanotechnology 22 (2011) 1–9, http://dx.doi.org/10.1088/0957-4484/22/1/015606, 015606.
[41] I.Y.Y. Bu, Novel all solution processed heterojunction using p-type cupric oxide and n-type zinc oxide nanowires for solar cell applications, Ceram. Int. 39 (2013) 8073–8078, http://dx.doi.org/10.1016/j.ceramint.2013.03.079.
[42] Z. Guo, D. Zhao, Y. Liu, D. Shen, J. Zhang, B. Li, Visible and ultraviolet light alternative photodetector based on ZnO nanowire/n-Si heterojunction, Appl. Phys. Lett. 93 (2008) 163501, http://dx.doi.org/10.1063/1.3003877.
[43] G. Amin, I. Hussain, S. Zaman, N. Bano, O. Nur, M. Willander, Current-transport studies and trap extraction of hydrothermally grown ZnO nanotubes using gold Schottky diode, Phys. Status Solidi Appl. Mater. Sci. 207 (2010) 748–752, http://dx.doi.org/10.1002/pssa.200925547.
[44] H.M. Chiu, Y.T. Chang, W.W. Wu, J.M. Wu, Synthesis and characterization of one-dimensional Ag-doped ZnO/Ga-doped ZnO coaxial nanostructure diodes, ACS Appl. Mater. Interfaces 6 (2014) 5183–5191, http://dx.doi.org/10.1021/am500470y.
[45] K.Y. Ko, H. Kang, J. Park, B.W. Min, H.S. Lee, S. Im, et al., ZnO homojunction core-shell nanorods ultraviolet photo-detecting diodes prepared by atomic layer deposition, Sens. Actuators A Phys. 210 (2014) 197–204, http://dx.doi.org/10.1016/j.sna.2014.02.005.
[46] K. Cheng, Q. Li, J. Meng, X. Han, Y. Wu, S. Wang, et al., Interface engineering for efficient charge collection in Cu2O/ZnO heterojunction solar cells with ordered ZnO cavity-like nanopatterns, Sol. Energy Mater. Sol. Cells 116 (2013) 120–125, http://dx.doi.org/10.1016/j.solmat.2013.04.021.
[47] F. Schuster, B. Laumer, R.R. Zamani, C. Magén, J.R. Morante, J. Arbiol, et al., P-GaN/n-ZnO heterojunction nanowires: optoelectronic properties and the role of interface polarity, ACS Nano 8 (2014) 4376–4384, http://dx.doi.org/10.1021/nn406134e.
[48] S.A. Chambers, T. Droubay, T.C. Kaspar, M. Gutowski, S.A. Chambers, T. Droubay, et al., Experimental determination of valence band maxima for SrTiO3, TiO2, and SrO and the associated valence band offsets with Si (001), J. Vac. Sci. Teknol. B 22 (2004) 2205–2215, http://dx.doi.org/10.1116/1.1768525.
[49] Z. Wang, C. Jia, Y. Chen, Y. Guo, X. Liu, S. Yang, et al., Valence band offset of InN/BaTiO 3 heterojunction measured by X-ray photoelectron spectroscopy, Nanoscale Res. Lett. 6 (2011) 1–5, http://dx.doi.org/10.1063/1.2839611.
[50] L. Chu, L. Li, W. Ahmad, Z. Wang, X. Xie, J. Rao, et al., Bandgap-graded ZnO/(CdS) 1-x (ZnS) x coaxial nanowire arrays for semiconductor-sensitized solar cells, Mater. Res. Express 1 (2014) 1–12, http://dx.doi.org/10.1088/2053-1591/1/1/015021.
[51] S.S. Wilson, Y. Tolstova, D.O. Scanlon, G.W. Watson, H.A. Atwater, W. Wu, et al., Cu2O/MgO band alignment and Cu2O-Au nanocomposites with enhanced optical absorption, Opt. Mater. Express 7 (2013) 3606–3610, http://dx.doi.org/10.1039/C4EE01956C.
[52] B. Kramm, A. Laufer, D. Reppin, A. Kronenberger, P. Hering, A. Polity, et al., Energy band alignment of SnO2/SrTiO3 epitaxial heterojunction studied by X-ray photoelectron spectroscopy ChangKe, a, Surf. Interface Anal. 100 (2015) 824–827, http://dx.doi.org/10.1063/1.3685719.
[53] P.D.C. King, T.D. Veal, A. Schleife, J. Zúñiga-Pérez, B. Martel, P.H. Jefferson, et al., Valence-band electronic structure of CdO, ZnO, and MgO from x-ray photoemission spectroscopy and quasi-particle-corrected density-functional theory calculations, Phys. Rev. B – Condens. Matter Mater. Phys. 79 (2009) 8–10, http://dx.doi.org/10.1103/PhysRevB.79.205205.
[54] E.A. Kraut, R.W. Grant, J.R. Waldrop, S.P. Kowalczyk, Semiconductor core-level to valence-band maximum binding-energy differences: precise determination by x-ray photoelectron spectroscopy, Phys. Rev. B 28 (1983) 1965–1977, http://dx.doi.org/10.1103/PhysRevB.28.1965.
[55] E.A. Kraut, R.W. Grant, J.R. Waldrop, S.P. Kowalczyk, Precise determination of the valence-band edge in X-Ray photoemission spectra: application to measurement of semiconductor interface potentials, Phys. Rev. Lett. 44 (1980) 1620–1623, http://dx.doi.org/10.1103/PhysRevLett.44.1620.
[56] M. Hussain, Z.H. Ibupoto, M.A. Abbassi, A. Khan, G. Pozina, O. Nur, et al., Synthesis of CuO/ZnO composite nanostructures, their optical characterization and valence band offset determination by X-Ray photoelectron spectroscopy, J. Nanoelectron. Optoelectron. 9 (2014) 348–356, http://dx.doi.org/10.1166/jno.2014.1594.
[57] A.K. Rana, Y. Kumar, P. Rajput, S.N. Jha, Search for origin of room temperature ferromagnetism properties in Ni doped ZnO nanostructure, ACS Appl. Mater. Interfaces 524 (2017), http://dx.doi.org/10.1021/acsami.6b12616.
[58] H. Naatz, S. Lin, R. Li, W. Jiang, Z. Ji, C.H. Chang, Safe – by – design CuO nanoparticles via Fe – doping, CuO bond length variation, and biological assessment in cells and zebrafish embryos, ACS Nano 11 (1) (2017) 501–515, http://dx.doi.org/10.1021/acsnano.6b06495.
[59] T. Hsueh, C. Hsu, S. Chang, P. Guo, Cu2O/n-ZnO nanowire solar cells on ZnO: Ga/glass templates, Scr. Mater. 57 (2007) 53–56, http://dx.doi.org/10.1016/j.scriptamat.2007.03.012.